THE ASTROPHYSICAL JOURNAL SUPPLEMENT SERIES, 154:10–17, 2004 September

THE INFRARED ARRAY CAMERA (IRAC) FOR THE *SPITZER SPACE TELESCOPE*

G. G. FAZIO,[1] J. L. HORA,[1] L. E. ALLEN,[1] M. L. N. ASHBY,[1] P. BARMBY,[1] L. K. DEUTSCH,[1,2] J.-S. HUANG,[1] S. KLEINER,[1] M. MARENGO,[1] S. T. MEGEATH,[1] G. J. MELNICK,[1] M. A. PAHRE,[1] B. M. PATTEN,[1] J. POLIZOTTI,[1] H. A. SMITH,[1] R. S. TAYLOR,[1] Z. WANG,[1] S. P. WILLNER,[1] W. F. HOFFMANN,[3] J. L. PIPHER,[4] W. J. FORREST,[4] C. W. MCMURTY,[4] C. R. MCCREIGHT,[5] M. E. MCKELVEY,[5] R. E. MCMURRAY,[5] D. G. KOCH,[5] S. H. MOSELEY,[6] R. G. ARENDT,[6] J. E. MENTZELL,[6] C. T. MARX,[6] P. LOSCH,[6] P. MAYMAN,[6] W. EICHHORN,[6] D. KREBS,[6] M. JHABVALA,[6] D. Y. GEZARI,[6] D. J. FIXSEN,[6] J. FLORES,[6] K. SHAKOORZADEH,[6] R. JUNGO,[6] C. HAKUN,[6] L. WORKMAN,[6] G. KARPATI,[6] R. KICHAK,[6] R. WHITLEY,[6] S. MANN,[6] E. V. TOLLESTRUP,[7] P. EISENHARDT,[8] D. STERN,[8] V. GORJIAN,[8] B. BHATTACHARYA,[9] S. CAREY,[9] B. O. NELSON,[9] W. J. GLACCUM,[9] M. LACY,[9] P. J. LOWRANCE,[9] S. LAINE,[9] W. T. REACH,[9] J. A. STAUFFER,[9] J. A. SURACE,[9] G. WILSON,[9] E. L. WRIGHT,[10] A. HOFFMAN,[11] G. DOMINGO,[11] AND M. COHEN[12]

Received 2004 March 26; accepted 2004 May 26

ABSTRACT

The Infrared Array Camera (IRAC) is one of three focal plane instruments on the *Spitzer Space Telescope*. IRAC is a four-channel camera that obtains simultaneous broadband images at 3.6, 4.5, 5.8, and 8.0 μm. Two nearly adjacent $5\farcm2 \times 5\farcm2$ fields of view in the focal plane are viewed by the four channels in pairs (3.6 and 5.8 μm; 4.5 and 8 μm). All four detector arrays in the camera are 256×256 pixels in size, with the two shorter wavelength channels using InSb and the two longer wavelength channels using Si:As IBC detectors. IRAC is a powerful survey instrument because of its high sensitivity, large field of view, and four-color imaging. This paper summarizes the in-flight scientific, technical, and operational performance of IRAC.

Subject headings: infrared: general — instrumentation: detectors — space vehicles: instruments

1. INTRODUCTION

The three *Spitzer Space Telescope* focal plane instruments were designed to investigate four major scientific topics: (1) the early universe, (2) brown dwarfs and superplanets, (3) active galactic nuclei, and (4) protoplanetary and planetary debris disks. Of these topics, the most important in defining the Infrared Array Camera (IRAC) design was the study of the early universe, and in particular the study of the evolution of normal galaxies to $z > 3$ by means of deep, large-area surveys. The 3–10 μm wavelength range was selected because stars have a peak emission at a wavelength of 1.6 μm, at the minimum of the H^- opacity (John 1988). The emission peak is a ubiquitous feature of stellar atmospheres and can be used to determine a photometric redshift for $1 < z < 5$ (Wright et al. 1994). The IRAC sensitivity requirement was set such that IRAC could achieve a 10 σ detection of an L^* galaxy at $z = 3$. This in turn required the measurement of a flux density at 8 μm of 8 μJy (10 σ; Simpson & Eisenhardt 1999). Channel 1 (3.6 μm) was selected to be at the minimum of the zodiacal background radiation (Wright 1985) and to avoid the water ice absorption band at 3.1 μm. The central wavelengths of the remaining IRAC filters and their bandwidths (approximately 25%) were then optimized (considering the detector materials available) to reach the sensitivity requirement and to permit the measurement of a photometric redshift for $1 < z < 5$ (Simpson & Eisenhardt 1999).

The number of individual channels in IRAC was limited by the number of array cameras that could fit in the specified volume. To reduce costs and maximize reliability, moving parts had to be minimized; hence, no filter wheels, only fixed filters, were used. Transmissive rather than reflective optics were used because of limited space. The pixel size was optimized to achieve the best point-source sensitivity for weak sources while maximizing the survey efficiency. The shutter at the entrance aperture was the only moving part allowed in IRAC.

Although the design was optimized for the study of the early universe, IRAC is a general-purpose, wide-field camera that can be used for a large range of astronomical investigations. In-flight observations with IRAC have already demonstrated that IRAC's sensitivity, pixel size, field of view (FOV), and filter selection are excellent for studying galaxy structure and morphology, active galactic nuclei, and the early stages of star formation and evolution and for identifying brown dwarfs.

IRAC was built by the NASA Goddard Space Flight Center (GSFC), with the Smithsonian Astrophysical Observatory (SAO) having management and scientific responsibility. Additional information on the operation and performance

[1] Harvard-Smithsonian Center for Astrophysics, 60 Garden Street, Cambridge, MA 02138; gfazio@cfa.harvard.edu.
[2] Deceased 2004 April 2.
[3] Steward Observatory, University of Arizona, 933 North Cherry Avenue, Tucson, AZ 85721.
[4] Department of Physics and Astronomy, University of Rochester, Rochester, NY 14627.
[5] NASA Ames Research Center, Moffett Field, CA 94035.
[6] NASA Goddard Space Flight Center, Laboratory for High Energy Astrophysics, Code 662, Greenbelt, MD 20771.
[7] Institute for Astronomy, 640 North A'ohoku Place, Hilo, HI 96720.
[8] Jet Propulsion Laboratory, California Institute of Technology, MS 264-767, 4800 Oak Grove Drive, Pasadena, CA 91109.
[9] *Spitzer* Science Center, MC 220-6, California Institute of Technology, Pasadena, CA 91125.
[10] Department of Physics and Astronomy, UCLA, P.O. Box 951562, Los Angeles, CA 90095.
[11] Raytheon Infrared Operations, 75 Coromar Drive, Building 2, MS 8, Goleta, CA 93117.
[12] Department of Astronomy, University of California, 601 Campbell Hall, Berkeley, CA 94720.

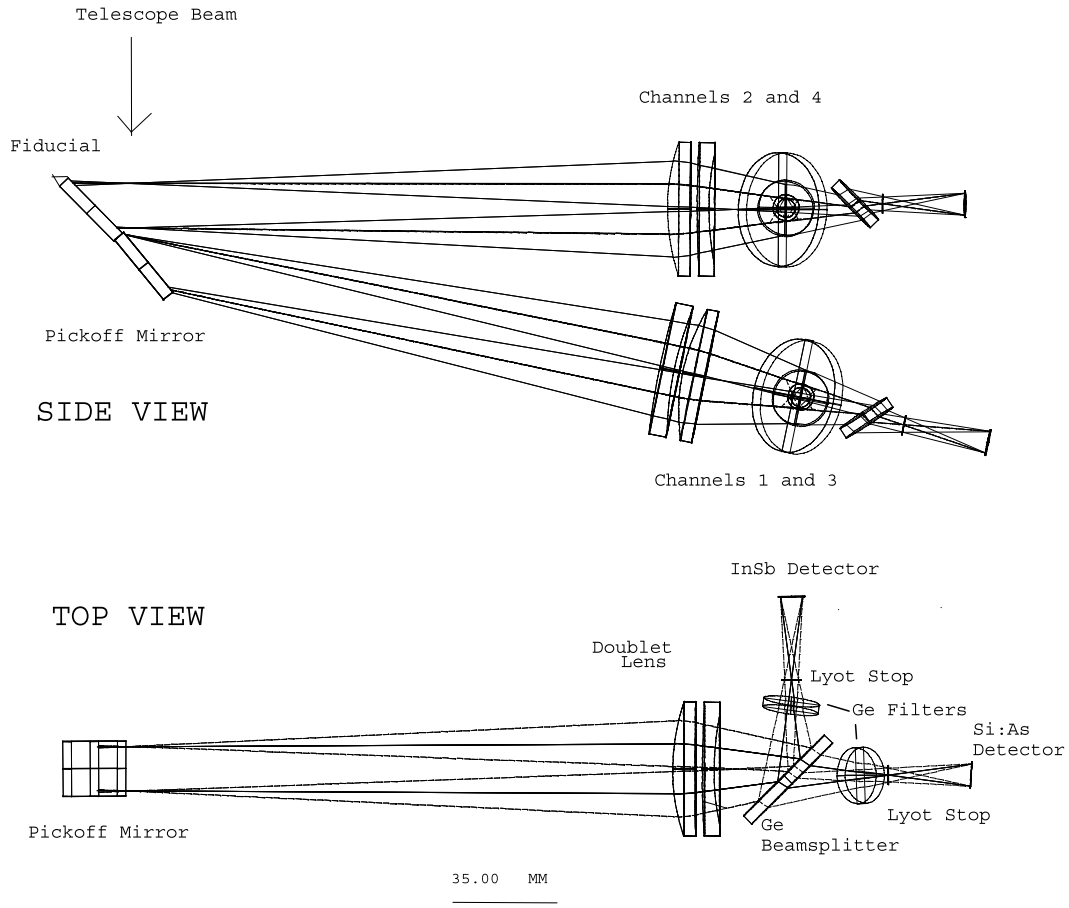

FIG. 2.—IRAC optical design, showing side view and top view.

of the IRAC instrument can be found at the IRAC Web site.[13]

2. INSTRUMENTATION DESCRIPTION

IRAC consists of two parts: the Cryogenic Assembly (CA), installed in the Multiple Instrument Chamber (MIC) within the Cryogenic Telescope Assembly (CTA), and the Warm Electronics Assembly (WEA), mounted below the CTA in the payload assembly area (Werner et al. 2004).

The IRAC CA, depicted in Figure 1 (Plate 1), consists of the following major subassemblies: two pick-off mirrors; the shutter; two optics housings, which hold the doublet lenses, beam splitters, filters, and cold stops; four focal plane assemblies (FPAs) that include the detector arrays and associated components; the transmission calibrator with its source and integrating spheres; and the housing structure, consisting of the main housing assembly and the wedge-shaped MIC adapter plate. The CA is cooled to the temperature of the MIC base plate ($\sim$1.2 K). The CA has a mass of 11.1 kg, is 0.15 m high and 0.28 m wide at its outer edge, and consumes an average of 3.0 mW of power during nominal operation.

The IRAC WEA resides in bay 5 of the spacecraft, operating at near room temperatures ($\sim 10^{\circ}$C). All electrical interfaces between the spacecraft and IRAC pass through the WEA. The WEA provides all power and data interfaces to both the spacecraft and to the CA as necessary to conduct the operation of IRAC. The WEA is connected to the CA via an extensive set of conventional and cryogenic cables, which pass through a junction box located on the spacecraft near the CTA. The junction box serves as the transition between the conventional and cryogenic cables.

The principal function of the WEA is the support and control of science data taking: the generation of bias voltages to the detectors; the timing of readout sequences; the amplification and digitization of the analog science signals; the digital signal processing of the images; and the transmission of the digital data to the spacecraft command and data handling (C&DH) solid-state recorders for mass storage, to be followed by downlinks to ground stations at 12 hr intervals. Apart from autonomous fault protection, the WEA internal software responds only to commands sent by the *Spitzer* C&DH computer. The WEA has a mass of 24.5 kg, and its dimensions are 0.46 m in length, 0.38 m in width, and 0.23 m in height. It consumes 56 W of power during nominal operation.

2.1. *Optical Design*

The IRAC optical path is shown in Figure 2. Light enters the CA via two pick-off mirrors located near the telescope focal plane. The two mirrors are slightly displaced and tilted to physically separate the optical components of the channel pairs. Thus, the pick-off mirrors project nearly adjacent $5\farcm2 \times 5\farcm2$ images of the sky to the channel pairs. The centers of the two images are separated by $6\farcm8$.

The lower mirror selects the field for channels 1 and 3. The reflected beam is incident upon an MgF_2-ZnS (Cleartran) vacuum-spaced doublet that reimages the *Spitzer* focal plane

[13] See http://cfa-www.harvard.edu/irac.

TABLE 1
IRAC Detector Characteristics

Channel	FPA Designation	Read Noise (e^-)	Quantum Efficiency (%)	Well Depth (e^-)	Operability (%)
1	48534/34 (UR)	8.1[a]	87	145000	99.97
2	48975/66 (GSFC)	6.8[a]	86	140000	99.99
3	30052/41 (ARC)	13.0[a]	45	170000	99.99
4	30219/64 (ARC)	6.6[b]	70	200000	99.75

[a] 200 s frame time.
[b] 50 s frame time.

onto the detectors. After the lenses, a germanium substrate beam splitter reflects the channel 1 beam and transmits the channel 3 beam. The beam splitter is tilted by 45° and is in the converging beam. The channel 1 light is reflected from the beam splitter and passes through a bandpass filter and then a Lyot stop, which rejects stray light. For channel 3, after the beam goes through the beam splitter, a filter selects the proper wavelength bandpass. The filter is tilted at 45°, in the plane opposite the beam splitter, to correct for the astigmatism introduced by the beam splitter. The situation is similar for channels 2 and 4, which are selected by the upper pick-off mirror. In these channels the doublet lens materials are ZnSe and BaF_2. The channel 2 beam is reflected by the beam splitter, and the channel 4 beam is transmitted. All filters are mounted on germanium substrates. The Lyot stops are oversized by 20%. Barr Associates, Inc., Westford, Massachusetts, produced the filters; OCLI-AJDS Uniphase Co., Santa Rosa, California, the beam splitters; and Spectral Systems, Inc., Dayton, Ohio, the lenses.

A shutter at the entrance to the CA was designed to block the incoming beams and to permit the measurement of the dark count rate of the detector arrays. A mirror, mounted on the rear surface of the shutter, reflects the light from the transmission calibration source into the two optical paths. To eliminate the possibility that the shutter could get stuck in the closed position, it has not been operated in flight to date.

IRAC has two internal calibration systems. The transmission calibration system measures IRAC optical throughput, and the flood calibrators test for detector responsivity and stability. Since the transmission calibration system requires that the shutter be closed, it has not been used in flight.

2.2. *Focal Plane Arrays*

The IRAC detector arrays were developed by Raytheon (SBRC), Goleta, California, under contract to SAO (Hoffman et al. 1998; Estrada et al. 1998). Channels 1 (3.6 μm) and 2 (4.5 μm) InSb detector arrays operate at a temperature of 15 K, and channels 3 (5.8 μm) and 4 (8.0 μm) Si:As detector arrays operate at 6 K. To help achieve the relative photometric accuracy requirement of 2%, the array temperatures are controlled by an active feedback circuit to less than 10 mK peak-to-peak variation from their set points. Both array types are 256×256 pixels in size and have the same physical pixel size of 30 μm. Cryo-CMOS technology was used in the readout multiplexer design (Wu et al. 1997). The arrays were antireflection coated with SiO for channels 1, 2, and 3 and with ZnS for channel 4. The power dissipation for each array during nominal operations is less than 1 mW. Table 1 lists some of the detector properties. The operability is the percentage of the pixels in an array that meet specifications.

The arrays can also be heated above their nominal operating temperatures to perform a thermal "anneal" of the FPAs to remove hot pixels or residual images. In the in-flight anneal operation, the temperatures of the FPAs are raised to 23 (channel 1) and 30 K (channels 2, 3, and 4) for approximately 2 minutes and then returned to their nominal operating temperatures in approximately 4 minutes.

The InSb arrays were tested and characterized at the University of Rochester (Pipher et al. 2000; Benson et al. 2000) and the Si:As arrays at the NASA ARC (McMurray et al. 2000). The flight arrays were evaluated at the NASA GSFC.

2.3. *IRAC Operation Mode*

IRAC has one method of operation on the *Spitzer Space Telescope*: stare and integrate. The FOV is determined by use of the full array (256×256 pixels) or the subarray (32×32 pixels) readout mode. Frame times for the full array can vary from 0.4 to 500 s in 0.2 s steps, but the times 2, 12, 30, 100, and 200 s are standard, except that channel 4 uses two or four 50 s frames instead of 100 and 200 s frames, respectively.

In the subarray mode, a 32×32 pixel region is read out at a faster rate. The standard frame times are 0.02, 0.1, and 0.4 s; other times can be commanded in steps of 10 ms. Each data collection command in subarray mode produces 64 image frames, taken consecutively with no dead time between frames. This mode is primarily for observing bright sources that would otherwise saturate the array or for observing time-critical events where a finer time resolution is required. This mode was used to measure the pointing jitter of the telescope.

During an integration, data are taken using a Fowler sampling method (Fowler & Gatley 1990) to reduce the effective read noise. This mode of sampling consists of taking N nondestructive reads immediately after the reset (pedestal levels) and another N nondestructive reads near the end of the integration (signal levels). The average of the pedestal levels is subtracted from the average of the signal levels to derive the signal. The averaging and subtraction of the two sets of reads are performed in the IRAC onboard electronics to generate a single image from each array, which is stored and transmitted to the ground. The N can vary from 1 to 64. The Fowler N used for an observation will depend on integration time and has been selected to maximize the signal-to-noise ratio (S/N) at each frame time, based on prelaunch performance tests.

IRAC is often used in a high dynamic range mode where a long exposure is preceded by one or more short exposures: 0.6, 12 s; 1.2, 30 s; 0.6, 12, 100 s; and 0.6, 12, 200 s. IRAC is capable of operating each of its four arrays independently and/or simultaneously. In normal flight operation, all four arrays are operated together.

TABLE 2
IRAC Point-Source Sensitivity (1 σ, μJy, Low Background)

Frame Time (s)	3.6 μm	4.5 μm	5.8 μm	8.0 μm
200	0.40	0.84	5.5	6.9
100	0.60	1.2	8.0	9.8
30	1.4	2.4	16	18
12	3.3	4.8	27	29
2	32	38	150	92
0.6[a]	180	210	630	250
0.4[b]	86	75	270	140
0.1[b]	510	470	910	420
0.02[b]	7700	7200	11000	4900

[a] High dynamic range mode.
[b] Subarray mode.

3. SENSITIVITY

The point-source sensitivities for the frame times available to IRAC are shown in Table 2. For each frame time and channel, the 1 σ sensitivity in μJy is given for the low-background case (near the ecliptic poles). The values were calculated based on the sensitivity model given by Hora et al. (2000), using measured in-flight values for the read noise, pixel size, noise pixels, background, and total system throughput. The numbers were compared to observations at several frame times to confirm the validity of the calculations. The values in Table 2 are close to preflight predictions of 0.5, 0.9, 3.1, and 5.0 μJy (1 σ, 200 s) for channels 1–4, respectively, except for the influence of two factors: the lower (better) than expected noise pixel values for all channels, and the lower (worse) throughput in channels 3 and 4. IRAC meets its required sensitivity limits of 0.92, 1.22, 6, and 9 μJy (1 σ, 200 s) for channels 1–4, respectively.

The noise measurements in channels 3 and 4 scale as expected with the inverse square root of time to the limit measured, 15,000 s. Channels 1 and 2 deviate from this rule in approximately 2000 s, which indicates that these channels are approaching the source completeness confusion limit (see also Fazio et al. 2004). The deviation occurs at about 1 μJy (5 σ), which is slightly fainter than the predictions for the IRAC confusion limit (Väisänen et al. 2001).

For extended emission in channels 3 and 4, the calibration was found to be significantly different than expected from the calibration derived from a point source. The calibration aperture (10 pixel radius; 12.″2 aperture radius) does not capture all of the light from the calibration sources so the extended sky emission appears too bright (Pipher et al. 2004). For photometry using different apertures, the estimated correction is listed in Table 6.4 of the *Spitzer* Observer's Manual.[14]

4. IRAC IMAGE QUALITY

IRAC's optics provides diffraction-limited imaging, with wave-front errors less than $\lambda/20$ in each channel. The in-flight IRAC image quality is limited by a combination of the optical quality of *Spitzer*, which is diffraction limited at 5.4 μm, and the size of the IRAC pixels. The predicted FWHM of the point-spread function (PSF), based on the preflight telescope and IRAC optical models, was 1.″6, 1.″6, 1.″8, and 1.″9 at 3.6, 4.5, 5.8, and 8.0 μm, respectively. Table 3 shows the properties of the IRAC PSF, derived from in-flight measurements of bright stars. The FWHM of the PSF will differ slightly for nonstellar spectra, e.g., dust. The PSF was monitored throughout the early mission while the telescope cooled down and while the secondary mirror was moved in two steps to achieve a near-optimal focus (Hoffmann et al. 2003). Column (2) in Table 3 gives the equivalent number of pixels whose noise contributes to noise in the analysis when an image is spatially filtered for optimum faint point-source detection (King 1983).

There are two columns for the FWHM of the PSF. The mean FWHM is from observations of a star at 25 different locations on the array. The FWHM for "centered PSF" is for cases where the star was most closely centered in a pixel. Column (5) in Table 3 is the percentage of the total flux in the central pixel for a point source that is well centered in a pixel. The flux in the central pixel for a random observation will be lower because the PSF of the telescope is rather undersampled at the IRAC pixel scale except in channel 4. The Strehl ratios observed are 0.37, 0.58, 0.62, and 0.95 for channels 1–4, respectively. The Strehl ratio for channel 3, after correction for scattered light in the array detector, is 0.71.

4.1. *Distortion*

There is a small amount of distortion over the IRAC FOV (Table 3). A quadratic distortion model is provided in the *Spitzer* Science Center (SSC) Basic Calibrated Data (BCD) pipeline, which fits in-flight data at rms $< 0.''2$ (channels 1 and 2) and rms $< 0.''3$ (channels 3 and 4) across the full arrays.

4.2. *Scattered and Stray Light*

Diffuse stray light from outside the IRAC FOV is scattered into the active region of the IRAC detectors in all four channels. The problem is more significant in channels 1 and 2 than in channels 3 and 4. In channels 1 and 2 the stray light pattern due to diffuse sources resembles a butterfly, while in channels 3 and 4 it resembles a tic-tac-toe board. A discussion of these effects and example images are given by Hora et al. (2004). These artifacts are due to zodiacal light scattered onto the arrays, possibly reflected from a hole in the FPA covers in channels 1 and 2 and from reflective surfaces outside the edges of channel 3 and 4 arrays. The stray light scales with zodiacal light, which is the light source for the flat fields, so the stray pattern contaminates the flats and all IRAC images. The "butterfly wings" have amplitudes of about 5% of the background intensity. The pipeline subtracts a model for the tic-tac-toe and butterfly patterns for the data, scaled based on a model for the zodiacal light intensity (Kelsall et al. 1998) at the location and time of the observation. To the extent the model is accurate, this corrects for the stray-light contamination.

Stars that fall in specific regions just outside the array edges scatter light into the detectors and produce distinctive patterns of scattered light on the array. Scattered light avoidance zones have been identified in each channel. Observers should avoid placing bright stars in these zones if their observations are sensitive to scattered light. Typically, in channels 1 and 2 about 2% of the light from a star is scattered into a "splatter pattern," which has a peak intensity of about 0.2% of the light from the star. The avoidance zones for channels 3 and 4 are a narrow strip about 3 pixels wide, 16 pixels outside of the array and surrounding it.

5. CALIBRATION

The overall requirement for the IRAC mission is that the system photometric responsivity be calibrated to a relative

[14] See http://ssc.spitzer.caltech.edu/documents/som.

TABLE 3
IRAC Image Quality

Channel (1)	Mean Noise Pixels (2)	Mean FWHM (arcsec) (3)	FWHM of Centered (arcsec) (4)	Peak Central Pixel Flux (%) (5)	Mean Pixel Scale (arcsec) (6)	Maximum Distortion[a] (pixels) (7)
1.....	7.0	1.66	1.44	42	1.221	1.3
2.....	7.2	1.72	1.43	43	1.213	1.6
3.....	10.8	1.88	1.49	29	1.221	1.4
4.....	13.4	1.98	1.71	22	1.220	2.2

[a] Maximum distortion in pixels relative to a square grid.

accuracy of 2% and that the absolute accuracy of the data set be determined to better than 10%. We expect that both of these requirements will be achieved. Currently 25% of the time that IRAC is on is devoted to calibration, but the excellent stability of IRAC will result in a significant decrease in that fraction.

5.1. *System Throughput and Isophotal Wavelength*

The IRAC system throughput and optical performance are governed by a combination of the system components, including the lenses, beam splitters, filters, mirrors, and detectors. Figure 3 gives the system throughput, including transmission of the telescope, IRAC optics, and quantum efficiency of the detectors (Hora et al. 2001; Stewart & Quijada 2000). For each IRAC channel, both polarizations were measured (Stewart & Quijada 2000), and the average polarization is shown by a solid curve.

The system parameters are summarized in Table 4. The isophotal wavelength $E(\lambda_{\rm isophotal})$ is the wavelength that must be assigned to the monochromatic flux density derived from a broadband measurement. The isophotal wavelength is defined as

$$E = \int_a^b E(\lambda)T(\lambda)\,d\lambda = E\left(\lambda_{\rm isophotal}\right)\int_a^b T(\lambda)\,d\lambda, \qquad (1)$$

where E is the measured in-band flux, $E(\lambda)$ is the irradiance at the entrance aperture of the telescope, $T(\lambda)$ is the spectral response of the system, and a and b define the wavelength range of interest. We calibrate the flux densities for a nominal spectrum $\nu I_\nu = \text{const}$. For source spectra with a range of slopes, $\alpha = d\log F_\nu/d\nu$ from -2 to $+2$, the color corrections are very close to unity (0.99–1.02). A color correction table for various values of the spectral index will be given in the *Spitzer* Observer's Manual.

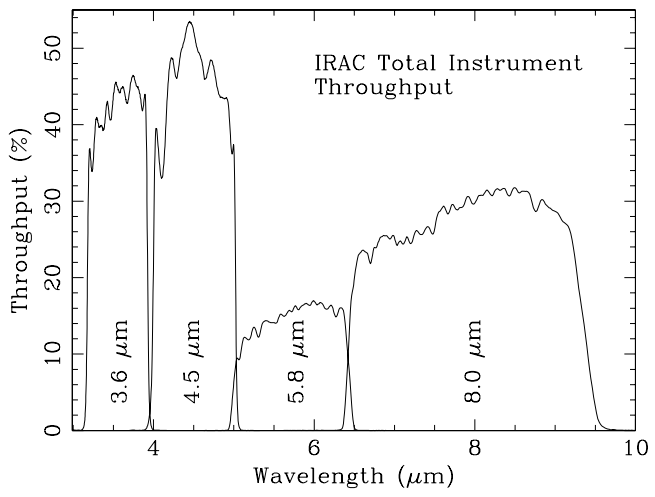

Fig. 3.—IRAC system total throughput, including transmission of the telescope, IRAC optics, and quantum efficiency of the detectors.

5.2. *Absolute Calibration*

A number of astronomical standard stars are observed in each instrument campaign to obtain a relative flux calibration (Megeath et al. 2001). Stars with a range of spectral indices and fluxes are observed at a number of positions across the array and many times throughout the mission to monitor any changes that may occur. To calculate Vega magnitudes from the calibrated IRAC images, use the zero-magnitude fluxes 277.5, 179.5, 116.6, and 63.1 Jy for channels 1, 2, 3, and 4, respectively. These fluxes were calculated from the IRAC throughput values and the absolute spectra at IRAC wavelengths (Cohen et al. 2003).

5.3. *Stability*

In-flight data indicate that IRAC is very stable; observations of calibration stars taken over 2 months are repeatable to about 2%.

5.4. *Linearity*

Both types of detectors have measurable nonlinearity. To linearize the data, a quadratic fit is used for the InSb arrays, and a cubic fit is used for the Si:As arrays. All arrays have been linearized to better than 1% up to approximately 90% of their full-well capacity. The detector linearity was measured during ground testing and verified during flight.

5.5. *Flat Field*

The flat field for each channel is defined as the factors by which one must correct each pixel to give the same value at a particular flux for uniform illumination. The factors include any field-dependent optical transmission effects, as well as the responsivity of the pixel and output electronics gain. Sky flats are obtained using a network of 24 high zodiacal background regions of the sky in the ecliptic plane, ensuring a relatively uniform illumination with a reasonable amount of flux. If the data are taken with an appropriate dither pattern, it is possible to relate the total response of each pixel to that of all others. One such region is observed at the beginning and end of each IRAC campaign. The data are reduced and combined to construct a flat-field image for each channel, which is then divided into the science data.

TABLE 4
IRAC Channel Characteristics

Channel	Isophotal λ[a] (μm)	Center λ[b] (μm)	Bandwidth[c] (μm)	Bandwidth[c] (%)	Average Transmission	Minimum In-Band Transmission	Peak Transmission
1.....	3.550	3.56	0.75	21	0.426	0.339	0.465
2.....	4.439	4.52	1.01	22	0.462	0.330	0.535
3.....	5.731	5.73	1.42	25	0.150	0.119	0.170
4.....	7.872	7.91	2.93	37	0.280	0.199	0.318

[a] The isophotal wavelength; see definition in text.
[b] The center wavelength is the midpoint between the points on the transmission curve that define the bandwidth.
[c] The bandwidth is the full width of the band at 50% of the average in-band transmission.

5.6. *Dark Frames, Offsets, and "First-Frame" Effect*

The detector dark currents are generally insignificant compared to the sky background. However, there is a significant offset or bias (which can be positive or negative) in a dark frame, which must be subtracted from the observations. Especially for shorter frames, the "dark" images are mostly due to electronic bias differences, rather than true dark current. Therefore, the number of electrons in a dark image does not scale linearly with exposure time. The shutter has never been used in flight, and therefore isolated dark/bias data cannot be taken. Instead, ground-based "lab" darks are used, in conjunction with sky darks that measure changes to the darks that have occurred since launch.

As part of routine operations a dark region of the sky near the north ecliptic pole is observed at the beginning and end of an IRAC campaign and every 3 days during the campaign. These data are reduced and combined in such a way as to reject stars and other astronomical objects with size scales smaller than the IRAC array. The resulting image of the minimal uniform sky background contains both the bias and the dark current. When subtracted from the routine science data, this will eliminate both of these instrumental signatures. The dark frames, when corrected for changes in the zodiacal background flux, remain very stable from campaign to campaign.

In general, the first frame of any sequence of images tends to have a different median value from other frames in the sequence, hence the name "first-frame effect." The smallest offsets occur when a frame is taken with a very short interval from the preceding image, which occurs when multiple frames are commanded at once. Such commands have been eliminated from IRAC science observations, so that there is always a finite interval between one frame and its predecessor. Since many IRAC observations will take only one image at each sky position and there is an 8–60 s delay while *Spitzer* points and settles to a new position, the first-frame effect is reduced significantly. The correction for the first-frame effect was derived from preflight ground-based data.

5.7. *Cosmic-Ray Effects*

In flight, cosmic rays excite approximately 3 pixels s^{-1} in channels 1 and 2 and approximately 5 pixels s^{-1} in channels 3 and 4. This is close to the predicted rate (Mason & Culhane 1983). The most common cosmic rays do not affect the pixel performance in subsequent frames and are confined to a few pixels around the peak. The cosmic-ray effects in channels 1 and 2 are more compact than those in channels 3 and 4, which have thicker detectors. In the latter channels the cosmic-ray effects appear as streaks and blobs. However, other events can cause streaks or other multiple-pixel structures in the array, and less common energetic and high-Z events can cause image artifacts in subsequent frames. Most of the cosmic-ray effects are removed by the post-BCD pipeline processing for observations that are well dithered.

On 2003 October 28, *Spitzer* encountered a large solar proton flare with an integrated dose of 1.6×10^9 protons cm^{-2} for proton energies greater than 50 MeV. IRAC was powered off at the time. After several thermal anneals of the arrays following the flare, only a few ($\sim$20) new hot pixels were detected, all in the channel 4 array.

6. ARTIFACTS OF THE IRAC ARRAYS

Array detector artifacts known before launch or discovered in flight include persistent images in channels 1 and 4, multiplexer bleed, column pull-down, and banding. These effects are described in more detail in the SSC Observer's Manual and in articles by Hora et al. (2000, 2001, 2003, 2004). To erase persistent images, both channels 1 and 4 are annealed simultaneously every 12 hr (after each downlink), and bright source observations are scheduled only near the end of an IRAC campaign. Column pull-down, bright source multiplexer bleed, and banding will be removed in the post-BCD pipeline corrections. The effects of persistent images and cosmic rays can be avoided or greatly reduced in observations that are well dithered. We recommend taking a minimum of three images of a science target in each channel as a best practice for observing with IRAC.

7. SUMMARY

In flight, IRAC meets all of the science requirements that were established before launch, and in many cases the performance is better than the requirement. IRAC is a powerful survey instrument because of its high sensitivity, large FOV, and four-color imaging from 3.2 to 9.5 μm wavelength. For example, in channel 1 (3.6 μm), IRAC can reach the same point-source sensitivity (19 mag, 5 σ, 1 hr) as the W. M. Keck telescope at 2.9–3.2 μm in only 1/100 the exposure time and does so with a far larger FOV: $5' \times 5'$ versus $40'' \times 40''$. In channel 4 (8.0 μm), IRAC can achieve the ultimate sensitivity limit reached by ISOCAM (15 μJy, 1 σ, 1 hr, $3' \times 3'$ field) on the *Infrared Space Observatory* (*ISO*) in the LW2 filter (6.7 μm) in approximately 1/100 the frame time (Alteri et al. 2000).

IRAC continues to function extremely well since the first images were produced, 7 days after launch, on 2003 September 1. The first scientific results of IRAC, which are presented in this issue, are examples of IRAC's great potential for producing exciting new science with the *Spitzer Space Telescope*.

Lynne Deutsch, a coauthor of this paper, died on April 2, 2004 after a long illness. Lynne was a dear friend and a close colleague. The IRAC team will deeply miss her presence. We dedicate this paper in her memory for all her contributions to infrared astronomy. This work is based on observations made with the *Spitzer Space Telescope*, which is operated by the Jet Propulsion Laboratory, California Institute of Technology under NASA contract 1407. Support for this work was provided by NASA through contract 125790 issued by JPL/Caltech. Support for the IRAC instrument was provided by NASA through contract 960541 issued by JPL.

REFERENCES

Alteri, B., Metcalfe, L., Blommaert, J., Elbaz, D., Starck, J.-L., & Aussel, H. 2000, Exp. Astron., 10, 291
Benson, R. G., Forrest, W. J., Pipher, J. L., Glaccum, W., & Solomon, S. L. 2000, Proc. SPIE, 4131, 171
Cohen, M., Megeath, S. T., Hammersley, P. L., & Stauffer, J. 2003, AJ, 125, 2645
Estrada, A. D., et al. 1998, Proc. SPIE, 3354, 99
Fazio, G. G., et al. 2004, ApJS, 154, 39
Fowler, A. M., & Gatley, I. 1990, ApJ, 353, L33
Hoffman, A. W., et al. 1998, Proc. SPIE, 3354, 24
Hoffmann, W. F., Hora, J. L., Mentzell, J. E., Trout-Marx, C., & Eisenhardt, P. R. 2003, Proc. SPIE, 4850, 428
Hora, J. L., et al. 2000, Proc. SPIE, 4131, 13
———. 2001, in The Calibration Legacy of the *ISO* Mission, ed. L. Metcalfe & M. F. Kessler (ESA SP-481; Noordwijk: ESA), 73
———. 2003, Proc. SPIE, 4850, 83
———. 2004, Proc. SPIE, 5487, in press
John, T. L. 1988, A&A, 193, 189
Kelsall, T., et al. 1998, ApJ, 508, 44
King, I. R. 1983, PASP, 95, 163
Mason, I. M., & Culhane, J. L. 1983, IEEE Trans. Nucl. Sci., NS-30, 485
McMurray, R. E., et al. 2000, Proc. SPIE, 4131, 62
Megeath, S. T., Cohen, M., Stauffer, J., Hora, J. L., Fazio, G., Berlind, P., & Calkins, M. 2001, in The Calibration Legacy of the *ISO* Mission, ed. L. Metcalfe & M. F. Kessler (ESA SP-481; Noordwijk: ESA), 165
Pipher, J. L., et al. 2000, Proc. SPIE, 4131, 7
———. 2004, Proc. SPIE, 5487, in press
Simpson, C., & Eisenhardt, P. 1999, PASP, 111, 691
Stewart, K. P., & Quijada, M. A. 2000, Proc. SPIE, 4131, 218
Väisänen, P., Tollestrup, E. V., & Fazio, G. G. 2001, MNRAS, 325, 1241
Werner, M., et al. 2004, ApJS, 154, 1
Wright, E. L. 1985, PASP, 97, 451
Wright, E. L., Eisenhardt, P., & Fazio, G. 1994, BAAS, 26, 893
Wu, J., Forrest, W. J., Pipher, J. L., Lum, N., & Hoffman, A. 1997, Rev. Sci. Instrum., 68, 3566

PLATE 1

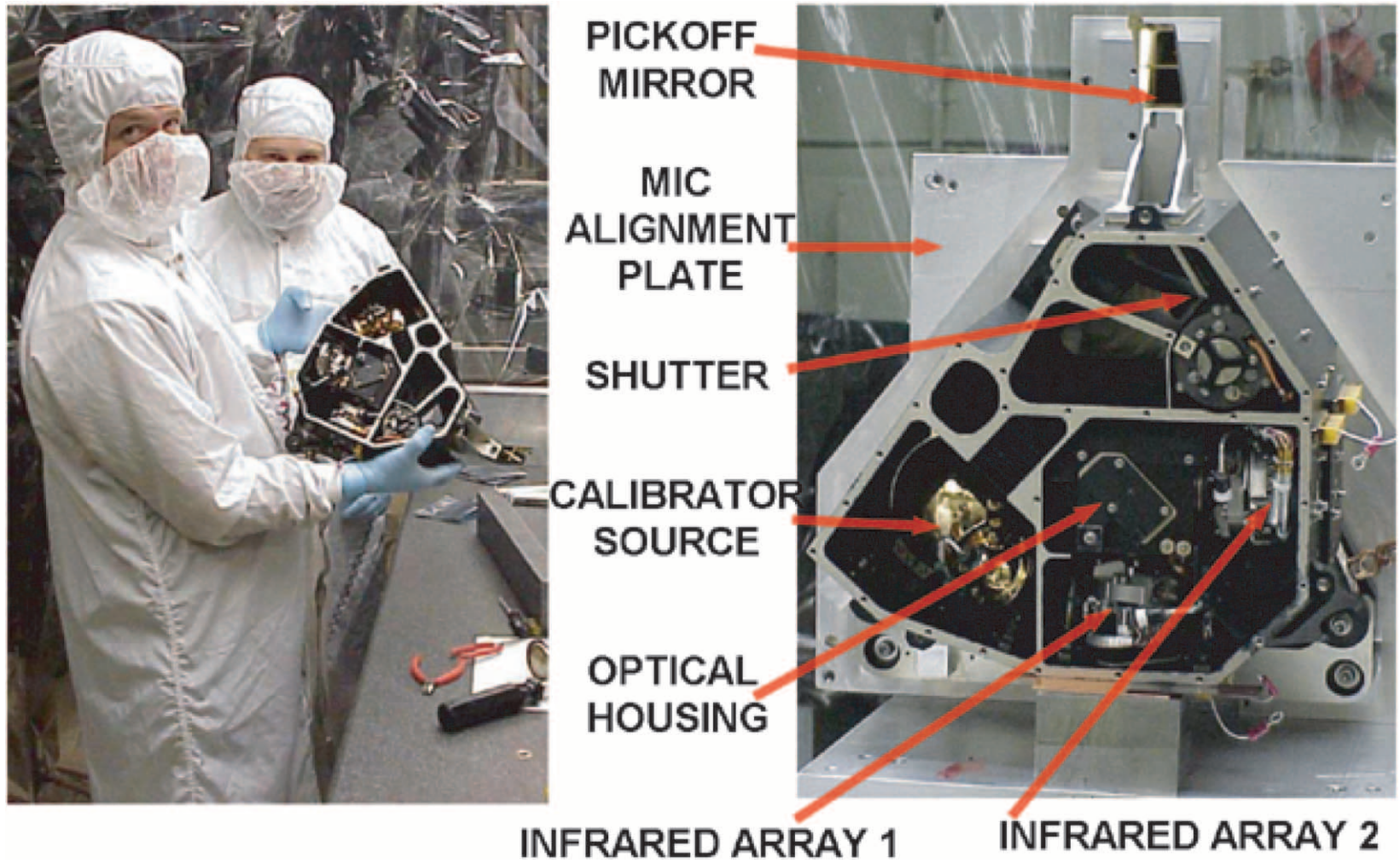

FIG. 1.—IRAC Cryogenic Assembly (CA) at NASA GSFC, with the top cover removed to show the inner components. The MIC alignment plate was used only for testing. The parts marked Infrared Array 1 and 2 are the IRAC channel 4 and 2 focal plane assemblies, respectively.